



OPEN ACCESS

EDITED BY

Manoj Khandelwal,
Federation University Australia, Australia

REVIEWED BY

Mohammad Azarafza,
University of Tabriz, Iran
Bailong Li,
Hebei University, China

*CORRESPONDENCE

Lijuan Zhang,
✉ zhanglijuan1969@126.com

RECEIVED 28 October 2025

REVISED 27 November 2025

ACCEPTED 29 November 2025

PUBLISHED 20 January 2026

CITATION

Zhang X, Xia C, Zhang L and Hou Z (2026)
Physical experimental study on the stability
analysis of granite residual soil slope with
boulder and dominant channel.
Front. Earth Sci. 13:1733802.
doi: 10.3389/feart.2025.1733802

COPYRIGHT

© 2026 Zhang, Xia, Zhang and Hou. This is an
open-access article distributed under the
terms of the [Creative Commons Attribution
License \(CC BY\)](https://creativecommons.org/licenses/by/4.0/). The use, distribution or
reproduction in other forums is permitted,
provided the original author(s) and the
copyright owner(s) are credited and that the
original publication in this journal is cited, in
accordance with accepted academic practice.
No use, distribution or reproduction is
permitted which does not comply with
these terms.

Physical experimental study on the stability analysis of granite residual soil slope with boulder and dominant channel

Xuesong Zhang¹, Chutian Xia², Lijuan Zhang^{3*} and Zhenkun Hou²

¹School of Architecture and Engineering, Guangzhou Polytechnic University, Guangzhou, Guangdong, China, ²School of Civil and Transportation Engineering, Guangdong University of Technology, Guangzhou, Guangdong, China, ³School of Smart city Engineering, Guangzhou Vocational University of Science and Technology, Guangzhou, Guangdong, China

Introduction: Granite residual soil exhibits pronounced engineering characteristics such as strong disintegration, high porosity, and structural heterogeneity, often containing compound structures of boulders and dominant seepage channels. This unique configuration leads to progressive instability and failure of slopes under rainfall infiltration.

Methods: To investigate this mechanism, a physical model testing system was established to analyze the stability characteristics and key influencing factors of granite residual soil slopes with boulders and dominant channels under rainfall conditions.

Results: The results show that the spatial position of boulders significantly regulates the evolution of the seepage field and the failure mode. Boulders located closer to the slope surface cause stronger local seepage deflection, concentrate the seepage path, accelerate shear zone formation, and enlarge the final landslide scale. The number of dominant seepage channels exerts a dual influence by forming rapid infiltration networks while inducing non-uniform soil saturation, resulting in a pronounced hydro-mechanical coupling effect that shortens slope stability time and increases landslide magnitude. In addition, higher soil compaction densifies the pore structure, reduces water migration, delays saturation, and thereby slows the development of instability.

Discussion: Although both boulders and dominant seepage channels promote slope instability, their mechanisms differ: dominant channels directly enhance internal water migration through preferential flow paths, whereas boulders indirectly induce new seepage pathways by altering the existing seepage field. Overall, this study elucidates the differential roles of boulders, dominant seepage channels, and soil compaction in rainfall-induced slope failure, providing a theoretical foundation for prevention and control.

KEYWORDS

boulder, dominant seepage channel, granite residual soil, influence factor, rainfall infiltration, slope

1 Introduction

Granite residual soil is an *in-situ* weathering deposit formed through the long-term physical and chemical weathering of granite parent rock under humid and hot climatic conditions. The soil is typically distributed in zonal patterns along the southeastern coast and in southern China. Its engineering characteristics include high porosity, significant structural heterogeneity, and strong hydrophilic disintegration (Wen et al., 2024; Lai et al., 2025; Liu et al., 2023), which have made it a key geological issue that urgently needs to be addressed in the field of slope engineering. The South China region, represented by Guangdong Province, has a typical subtropical monsoon climate characterized by high annual precipitation and seasonally concentrated rainfall. Granite residual soil slopes, featuring well-developed multi-scale pore structures and commonly containing large isolated boulders and dominant seepage channels, are prone to the formation of transient saturation zones under continuous rainfall. These conditions can easily induce progressive landslides and associated rockfall hazards (Pan et al., 2020; Tan et al., 2025; Wu et al., 2022; Chen et al., 2025). This complex disaster mode poses a serious threat to regional infrastructure and the safety of local residents. Therefore, conducting a systematic study on the stability of granite residual soil slopes containing isolated boulders and dominant seepage channels under rainfall conditions is of great theoretical and practical significance for improving slope disaster early-warning systems and optimizing the design of protective engineering measures (Yu et al., 2023; Zhao et al., 2024; Mao et al., 2024; Li et al., 2022).

The rainfall-induced instability of granite residual soil slopes demonstrates a pronounced geological disaster chain, often leading to significant consequences from compound landslide-debris flow events, which represents a key scientific problem in geotechnical engineering (Pradhan and Kim, 2015; Bai et al., 2022; Lan et al., 2025). Significant efforts have been made by the global research community to tackle this problem, leveraging interdisciplinary approaches for a systematic investigation. Studies have demonstrated that rainwater infiltration through preferential flow paths facilitates shallow failure, thereby accelerating the overall instability of slopes (Tao et al., 2017). Furthermore, vegetation can enhance the overall permeability of soil, but the gap between its roots and soil may also evolve into a dominant infiltration channel, accelerating rainwater infiltration under heavy rainfall, forming a potential slip surface, and inducing landslides (Wang R et al., 2023; Hang et al., 2023). Analyses on the mechanism of preferential seepage indicate that it significantly influences soil moisture content and pore water pressure, which are critical factors in triggering landslides (Liu et al., 2020; Jian et al., 2020; Ling et al., 2023; Shu et al., 2023).

In summary, a similarity-based physical model of the slope incorporating boulder distribution and dominant channel development was established, which elucidates the progressive failure mechanism of granite residual soil slopes under coupled seepage–stress conditions (Feng et al., 2022; Li et al., 2025; Guo et al., 2023). In numerical simulation aspects, a multiscale analysis model integrating the discrete element and finite element methods was established, enabling dynamic simulation of the coupled processes of rainfall infiltration, soil softening,

and slip surface evolution (Xu, 2023; Dou et al., 2024; Bravo-Zapata et al., 2022). In terms of theoretical research, a slope stability criterion considering the mechanical properties of unsaturated soils was proposed, thereby improving the theoretical framework for predicting rainfall-induced landslides (Wang Y et al., 2023; Liu et al., 2024; Ding et al., 2023). In terms of disaster-causing mechanisms, this study focused on the chain reaction process of rainfall infiltration, pore water pressure evolution, and soil strength degradation. It clarified the interaction between pore water pressure fluctuations and soil strength deterioration, and revealed the regulatory mechanism of dominant channels on the distribution of the seepage field (Bai et al., 2021; Liu et al., 2022). At the level of protective measures, this study proposed and developed a comprehensive prevention and control system centered on a three-dimensional drainage structure and integrated with ecological slope protection technology. Through the synergistic effects of multi-dimensional drainage pathways and vegetation reinforcement, the system effectively reduced the accumulation of pore water pressure within the slope and improved the shear strength of the soil, thereby significantly enhancing the long-term stability and ecological sustainability of the slope (Wang Z et al., 2023; Rahardjo et al., 2023; Wang et al., 2025). In summary, based on the revealed coupling evolution mechanism of seepage and stress and the multi-factor synergistic failure process in granite residual soil slopes, this study proposes a comprehensive prevention and control system centered on three-dimensional drainage and ecological slope protection. The research outcomes not only deepen the understanding of the formation mechanism of rainfall-induced landslides but also provide essential theoretical support and practical engineering guidance for the stability control of granite residual soil slopes.

However, the synergistic effect of boulders and dominant channels can significantly reshape the seepage field distribution within a slope. The formation of this heterogeneous seepage structure accelerates the progressive failure process and adversely affects overall slope stability. Nevertheless, the quantitative relationships among key parameters—such as the spatial distribution of boulders, the number of dominant channels, and the degree of soil compaction—remain insufficiently interpreted, and their underlying mechanisms are still unclear.

Therefore, this study conducts a series of indoor model tests on granite residual soil slopes containing boulders and dominant channels under rainfall conditions. By controlling critical parameters including the buried position of boulders, the number of dominant channels, and the compaction degree of the slope, the dynamic evolution of soil moisture during failure is synchronously and continuously monitored. Based on the morphological analysis of different failure modes, this work explores the coupling mechanism between the seepage and stress fields and reveals the synergistic effects of boulder distribution, dominant channel development, and soil compaction on slope stability.

2 Physical model experimental device and experimental scheme

In order to investigate the failure mechanisms of granite residual soil slopes with isolated stones and preferential flow paths under

rainfall infiltration, as well as to explore the dynamic evolution of soil moisture content, infiltration rate characteristics, and the progressive failure response under various initial conditions, this study independently developed a physical model test system for analyzing the stability of such slopes. The core function of this system is to quantitatively analyze the driving mechanisms of rainfall infiltration in the process of slope instability and disaster initiation. Designed with a modular approach, the experimental setup primarily consists of three functional units: (1) a boundary-constrained model test box; (2) an artificial rainfall simulation system capable of precise rainfall control; and (3) an image analysis system integrating multi-source data acquisition and slope deformation monitoring. Through multi-physics coupling monitoring, this apparatus comprehensively captures the response characteristics of the entire slope failure process, from changes in the seepage field to progressive failure.

2.1 Experimental device

2.1.1 Modular experimental model box

The test model box was designed with standardized dimensions of 97 cm × 47 cm × 70 cm and consists of a metal frame, soil-bearing unit, and drainage control system. The frame, fabricated from high-strength stainless steel, provides sufficient rigidity to resist lateral earth pressure and maintain structural stability during testing. A transparent acrylic side wall, sealed with specialized sealant, allows direct observation of the slope failure process. The drainage system includes a floor drain with a multilayer filter and side-wall drain holes to prevent blockage by fine particles. To minimize boundary effects, a low-friction transparent film was attached to the inner wall, reducing contact resistance between the soil and box wall. Additionally, a supporting metal frame of the same material was installed to secure the artificial rainfall device and position the rainfall curtain.

2.1.2 Artificial rainfall system

The model box and artificial rainfall device are shown in Figure 1. As a key device for simulating natural rainfall, the structural design and parameter control of the artificial rainfall system are critical to the accuracy of experimental results. The system adopts a modular design and consists of three main components: a water supply unit, a water delivery unit, and a rainfall unit. Its core components include a constant-pressure water supply device, PE delivery pipelines, precision flow-regulating valves, a high-pressure atomization pump set, adjustable rainfall supports, and porous atomization nozzles. Municipal tap water was used as the water source, and its quality had negligible influence on soil infiltration. Rainfall intensity was dynamically controlled by the precision flow-regulating valve in conjunction with the constant-pressure pump, ensuring that the target rainfall rate could be achieved and maintained. Rainfall duration was managed by an electronic timing controller, enabling the system to operate in either continuous rainfall mode or a variable-pulse mode. In this study, a steady-state rainfall condition was adopted to simulate prolonged heavy rainfall events, while the system is also capable of producing intermittent rainfall pulses when required by other experimental scenarios. To simulate the physical characteristics of natural rainfall, high-pressure atomization

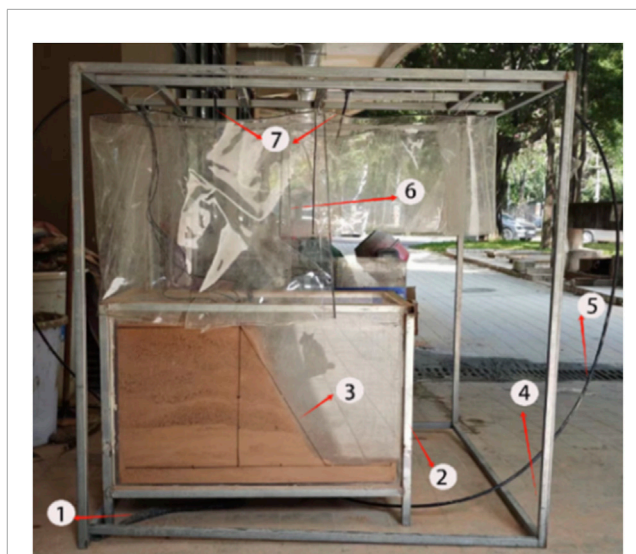


FIGURE 1
Model box and artificial rainfall device (① Floor drain system; ② Inner metal frame; ③ Model box body; ④ Outer metal frame; ⑤ PE water pipe; ⑥ Rain curtain; ⑦ Atomizing nozzle).

technology was employed to generate fine, controllable water droplets, effectively eliminating splash effects typical of traditional droplets. The atomizing nozzles were installed 62 cm above the model box in a circular array, with an effective spray diameter of approximately 40 cm, ensuring uniform rainfall distribution on the slope surface. To minimize environmental interference, a weatherproof curtain was installed around the apparatus to block wind disturbance, prevent water splash from affecting sensors, and maintain a controlled experimental environment.

2.1.3 Data and image acquisition device

As shown in Figure 2, a multi-source data fusion acquisition system was employed in this experiment. The hardware configuration includes a distributed moisture content sensor array, a pore water pressure monitoring network, an earth pressure sensing unit, a high-resolution camera system, a static signal acquisition and analysis platform, a data relay gateway, and a central processing terminal. Soil moisture evolution was monitored using capacitance-based moisture sensors, which operate on a dielectric measurement principle similar to TDR and provide continuous volumetric water content readings. This enables real-time tracking of the spatial and temporal development of soil saturation during rainfall infiltration. Pore-water pressure transducers installed at key monitoring positions captured the hydraulic response of the interior seepage field, while earth pressure cells recorded stress redistribution associated with wetting-induced softening. The image acquisition system adopts a dual-stand layout, with industrial cameras positioned on the front and side elevations of the model box. Although digital image correlation was not applied in this study, the synchronized high-frame-rate imaging provides continuous visual documentation of slope deformation and aids interpretation of near-surface wetting front migration. All sensor signals were filtered and amplified by the static testing and analysis platform, then transmitted to the computer terminal via the data gateway,

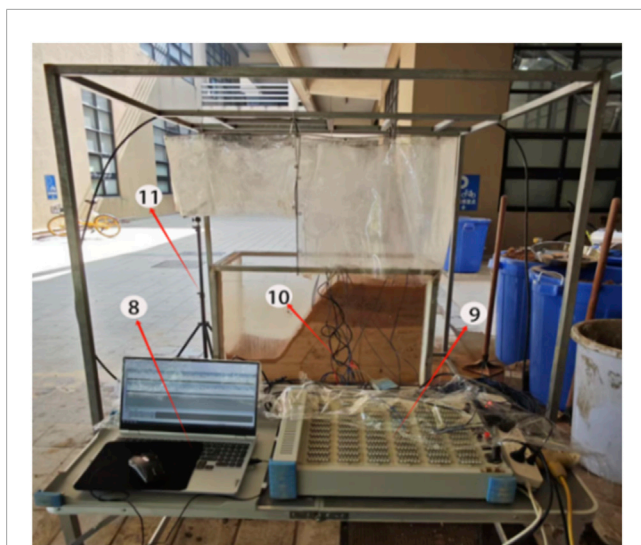


FIGURE 2
Data and image acquisition system (Ⓒ Computer, Ⓓ data acquisition instrument, Ⓔ soil moisture sensor Ⓕ image acquisition instrument).

forming a digital monitoring system that captures the coupling behavior of multiple physical fields.

2.2 Experimental scheme

2.2.1 Fill and rainfall design

The prototype slope used in this experiment is located at the construction site of Phase II of the Jinwan District Grain Depot in Dahuan Village, Kuangshan Community, Hongqi Town, Zhuhai City. The surrounding terrain is characterized by a straight slope with a toe length of approximately 11 m, a height of 12 m, and a relatively steep inclination of about 60°. A small number of boulders are scattered across the slope surface, and no faulted or fractured zones were identified, indicating that the rock mass is generally intact. Due to rainfall erosion, localized collapses were observed near the slope toe; however, under natural conditions, the overall slope remains generally stable along its length.

Based on similarity theory (Abgrami et al. 2025; Moazafarbaygi and Asghari-Kaljahi, 2024; Danesh et al. 2025), a geometric similarity ratio of 22.6 was adopted for the physical model tests. Accordingly, a granite residual soil slope model with dimensions of 78.6 cm in length, 48 cm in width, and 53 cm in height was constructed, maintaining the same slope angle of 60°.

This study adopts a controlled variable experimental design comprising three groups of comparative tests to investigate the influence mechanisms of boulder spatial distribution, dominant seepage channel development, and soil compaction on slope stability under rainfall infiltration. The test variables include: ① spatial position of boulders; ② number gradient of dominant channels; and ③ soil compaction level. A distributed soil moisture sensor array was installed to continuously monitor the spatiotemporal evolution of the soil moisture field in real time. By comparing the results of multiple test groups, the effects of different control factors on slope stability were systematically analyzed. The experimental design is

based on similarity theory, combined with the actual site conditions, the physical and mechanical properties of the soil, and the geometric constraints of the model box, while fully considering boundary effects and particle-scale interactions. The specific design details are as follows:

The design of the test parameters was based on statistical analysis of historical rainfall data from the Pearl River Delta, with a rainfall intensity of 120 mm/h selected as the control index. A stable head pressure was maintained using a high-pressure water pump system, and rainfall intensity was precisely regulated through a precision flow control device. Prior to formal testing, the rainfall system was standardized and calibrated through ten parallel tests. The results indicated that the relative deviation between the measured and target rainfall intensities ranged from 3.1% to 4.5%, which is within an acceptable error range.

The soil material used in the test was granite residual soil, with initial physical properties as follows: dry density of 1.28–1.76 g/cm³ and volumetric moisture content of 18%–24%. Based on the mechanical properties of undisturbed soil, the dry density of the remolded soil was controlled at 1.70 g/cm³, and the moisture content was adjusted to 22%. All samples were pretreated to remove impurities such as weeds, gravel, and industrial debris. The slope model was constructed using a layered compaction process. Specifically, remolded soil was filled in 15 cm layers, and after each compaction, three samples were collected from representative locations using the standard ring-knife method to verify that the dry density met the control value. Soil compaction was quantified as the ratio of achieved dry density to the target value ($\rho_d/\rho_{d,target}$), and compaction passes were repeated until this ratio fell within $\pm 2\%$ of the target. Interlayer bonding surfaces were roughened with a scraping tool to enhance mechanical interlocking between layers. During filling, boulders were embedded at predetermined spatial coordinates according to the experimental design. Upon completion of filling, mechanical excavation combined with manual trimming was performed to shape the slope, forming a final geometry with a design inclination of 60°. The physical and mechanical parameters of the soil used in the test are listed in Table 1.

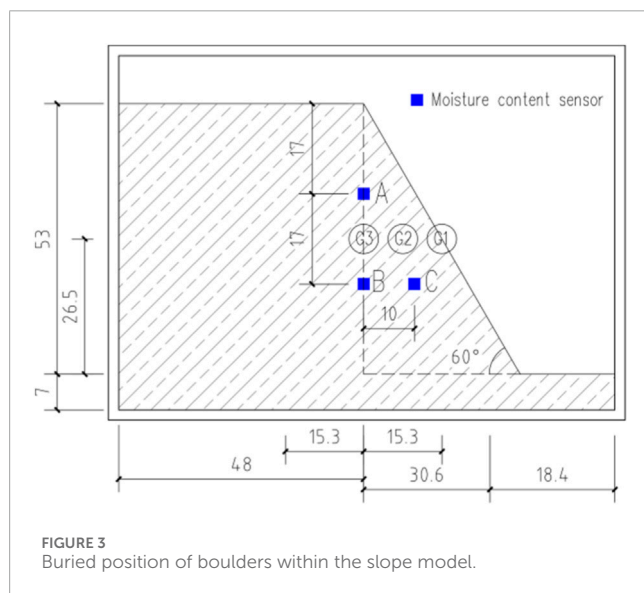
2.2.2 Test scheme for influence of boulder on stability of granite residual soil slope

As shown in Figure 3, this study employs a physical model test to systematically investigate the influence mechanism of boulders on the stability of granite residual soil slopes. By designing slope models with varying boulder distribution characteristics and conducting laboratory simulations, the effects of boulder spatial distribution, geometric shape, and content on slope stability parameters were quantitatively analyzed, revealing the instability mechanism under boulder–soil interaction.

The boulders at the construction site exhibit irregular geometries. To ensure the reliability and controllability of the physical model, geometric symmetry was required for the modeled boulders. The *in-situ* boulders measure approximately 120.6–150.6 cm in length, and an average value of 135.6 cm was adopted for scaling. Based on the previously established geometric similarity ratio of 22.6, marble spheres with a diameter of 6 cm were ultimately selected as the model boulders. The geometric symmetry of the spheres provides dual verification for model reliability: the

TABLE 1 Index parameters of soil used in the test.

Parameter index	Cohesion c_p/kpa	Internal friction angle $\varphi/(\circ)$	Modulus of deformation E_p/Gpa	Poisson's ratio μ
Numerical value	16	21	5.4	0.25



left–right data consistency and the ability to highlight general failure patterns.

As shown in Table 2, four groups of slope models were tested, where Group G1 served as the control without boulders, and the remaining groups each contained a single embedded boulder. To eliminate the influence of material water absorption on rainfall infiltration, all boulders were pre-saturated in water for 48 h before placement. The monitoring layout included a distributed soil moisture sensor array, a pore water pressure network, and precisely embedded earth pressure boxes, as detailed in the plan view of Figure 4 and the coordinate parameters in Table 2.

2.2.3 Test scheme for influence of dominant seepage channels development on slope stability in granite residual soil

As shown in Figure 4, vertical preferential seepage channels were installed at different locations along the model slope surface. To facilitate a clearer comparison of the respective influences of boulders and preferential flow channels on slope behavior, the geometric parameters of the channels were uniformly designed with a diameter of 1 cm and a depth of 6 cm.

The experiment adopted the control variable method, in which Group G4 served as the blank control without dominant seepage channels. The spatial layout parameters of the infiltration channels and sensors for Groups G4–G6 are listed in Table 3 (note: lowercase letters denote infiltration channel numbers, while uppercase letters represent sensor numbers). By varying the number of dominant seepage channels as the key control parameter, three groups of

comparative tests were conducted to quantitatively analyze the influence of channel development on the slope seepage field.

2.2.4 Test scheme for influence of soil compaction on stability of granite residual soil slope with boulders

In this study, a comparative testing approach was adopted to construct two slope models with different compaction levels. The dry density of the low-compaction group (G3) was controlled at 1.10 g/cm^3 , while that of the high-compaction group (G7) was maintained at 1.70 g/cm^3 . In both tests, boulders were embedded at fixed positions—30.6 cm from the slope toe and 26.5 cm from the slope crest. The compaction difference was achieved through a layered compaction process: the high-compaction model employed a 10 cm layer thickness with 10 compaction passes per layer, whereas the low-compaction model used a 15 cm layer thickness with 5 compaction passes per layer. Although microstructural characterization (e.g., pore-size distribution) was not conducted, the macroscopic control of dry density and compaction allows interpretation of the delayed failure onset in the high-compaction slope, as denser packing and stronger interlayer bonding reduce water infiltration rates and prolong the time to local instability.

The quantitative evaluation of the influence of boulder position and seepage channel number was performed using a parametric comparative method. Each test group varied only one key parameter, allowing the isolation of its individual contribution to the hydraulic and mechanical response. Subsequent analysis of infiltration rate, pore-water pressure evolution, and local instability timing enabled the establishment of empirical relationships linking boulder position, channel number, and slope instability indicators. These empirical trends provide a quantitative basis for interpreting the combined influence of internal structural heterogeneity on seepage-field evolution.

3 Analysis of test results

3.1 Influence of boulders on stability of granite residual soil slope

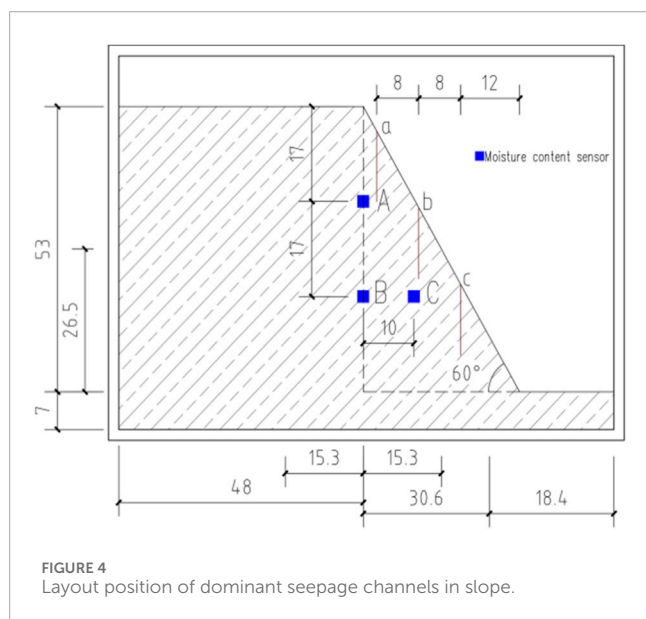
3.1.1 Influence of boulders on failure mode

As shown in Figure 5, the progressive failure processes of slopes G1, G2, and G3 under different rainfall durations were recorded. In the G1 test, the boulder was exposed on the slope surface, whereas in G2 and G3, the boulders were embedded within the slope body. After 360 min of continuous rainfall, no macroscopic landslides occurred in any of the three test groups.

During the pre-rainfall period, the slope primarily experienced surface flow erosion. Rainwater accumulated at the crest and flowed

TABLE 2 Distribution table of buried location of boulders.

Test number	Vertical distance between boulder and slope top (cm)	Horizontal distance between boulder and slope toe (cm)
G1	26.5	15.3
G2	26.5	22.95
G3	26.5	30.6



downslope, scouring and selectively transporting loose soil particles. The G1 slope exhibited pronounced surface erosion, with rainwater carrying fine particles downward, eventually causing the boulder to migrate and fall to the slope toe. In contrast, the G2 and G3 slopes showed localized instability near the crest, where tension cracks began to develop.

During the middle stage of rainfall, surface erosion intensified as scratches and rills increased. Cracks at the slope crest extended laterally and deepened, leading to small-scale soil detachment. The G1 slope exhibited multiple cracks that developed rapidly at the crest, ultimately resulting in overall slope instability. The G2 slope failed primarily through erosion along surface cracks induced by runoff, while the G3 slope showed continuous crack propagation behind the crest without global instability.

During the late stage of rainfall, large-scale landslide damage occurred due to the downward movement of soil along slope cracks. The G1 slope experienced a major landslide, the G2 slope showed overall instability with boulder exposure on the slope surface, and the G3 slope experienced a smaller-scale landslide with largely stable slope body. These results indicate that the location of boulders significantly affects the speed and scale of slope instability: boulders closer to the slope surface accelerate instability and increase damage scale, providing a basis for rainfall stability evaluation.

3.1.2 Influence of boulders on water content

As shown in Figure 6, the variation in soil moisture content during the progressive failure process of slopes G1, G2, and G3 was monitored under different rainfall durations. Sensor A was positioned above the boulder, while sensors B and C were installed below it. The moisture contents at locations A and C, both situated near the slope surface, increased rapidly due to direct exposure to infiltrating rainwater. In contrast, the moisture content at location B, positioned deeper within the slope, remained relatively constant during the early rainfall stage owing to limited infiltration. As rainfall continued, the moisture content at this location gradually increased, while in the later stage, the rate of increase slowed as the soil approached saturation.

By comparing and analyzing the moisture content data from the three test groups, it was found that the G2 slope exhibited the highest moisture content at all three monitoring locations. At locations A and B, the moisture content of the G3 slope was higher than that of the G1 slope, whereas at location C, the G1 slope showed a higher moisture content than the G3 slope.

From the moisture content variation curves of the slopes containing boulder, it can be observed that the presence of boulder form dominant seepage channel within the slope, thereby accelerating the downward migration of rainwater. In the G1 slope, where the boulder is located on the surface, the internal moisture content remains the lowest due to limited infiltration into deeper layers. In contrast, the boulder in the G2 slope is positioned between sensors B and C, allowing rainwater to bypass the boulder and infiltrate downward along its sides, resulting in the highest overall moisture content among the three test groups.

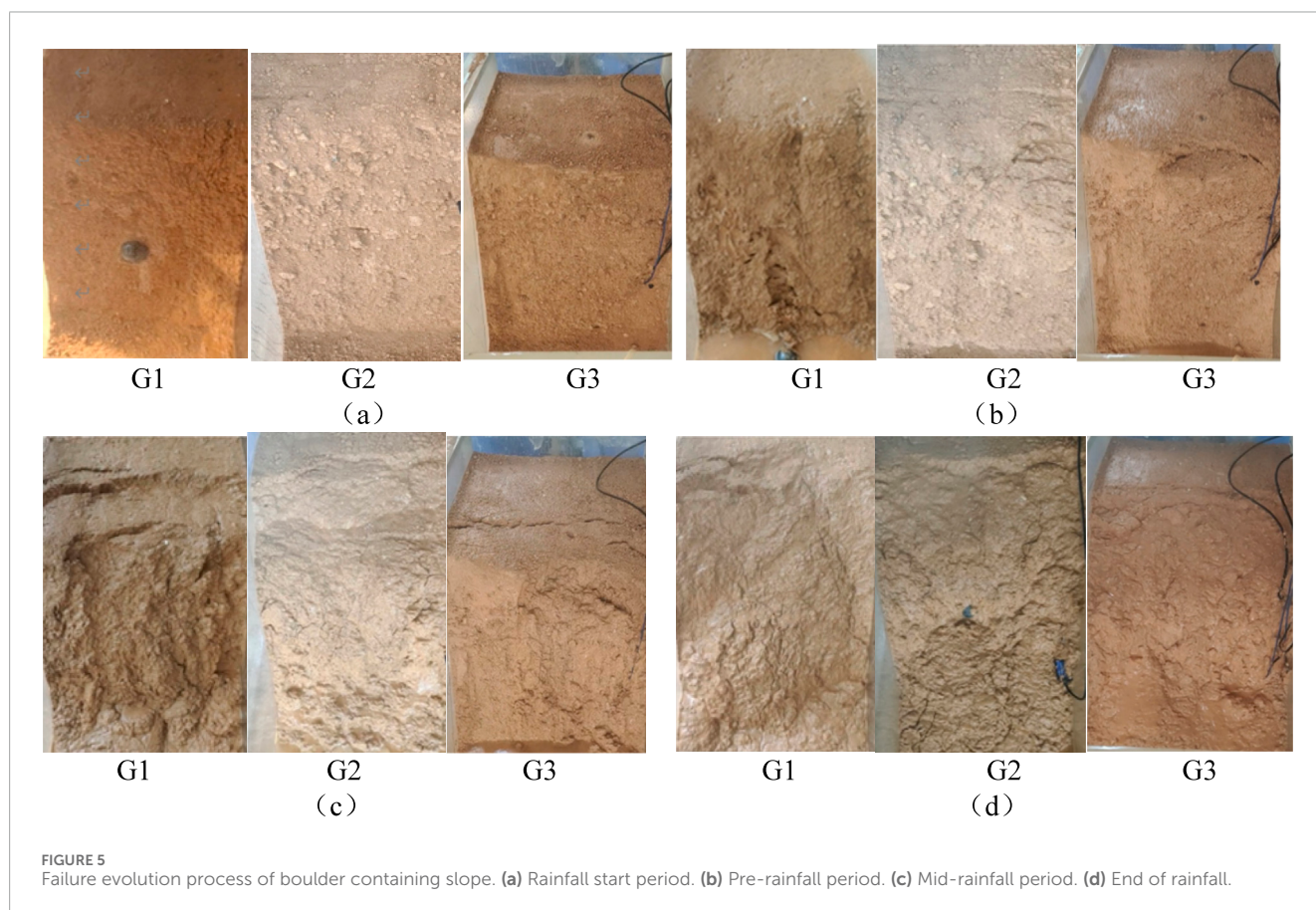
3.2 Influence of dominant seepage channels on stability of granite residual soil slope

3.2.1 Influence of dominant seepage channels on failure mode

As shown in Figure 7, the progressive failure processes of slopes G4, G5, and G6 were recorded under different rainfall durations. The G4 test served as a blank control without dominant channels, whereas the G5 and G6 tests were designed with one and three dominant channels, respectively, each 6 cm deep and located on the slope surface. After 240 min of continuous rainfall, no significant landslides occurred, marking the completion of the experiments.

TABLE 3 Distribution of dominant seepage channels.

Test number	Layout position of dominant channel	Depth of dominant seepage channel (cm)
G4	—	—
G5	b	6
G6	a, b, c	6



During the pre-rainfall stage, the infiltration capacity of the unsaturated granite residual soil exceeded rainfall intensity, allowing rapid absorption of most rainwater. Rainwater infiltrated quickly into the slope through the dominant seepage channels. The toe of the G4 slope exhibited slight softening, with no significant damage or cracking at the crest. In the G5 slope, cracks developed along the dominant channel, and soil near the crest showed downward sliding tendencies. In the G6 slope, “U”-shaped failure cracks formed near the two dominant channels, accompanied by ponding at the slope toe.

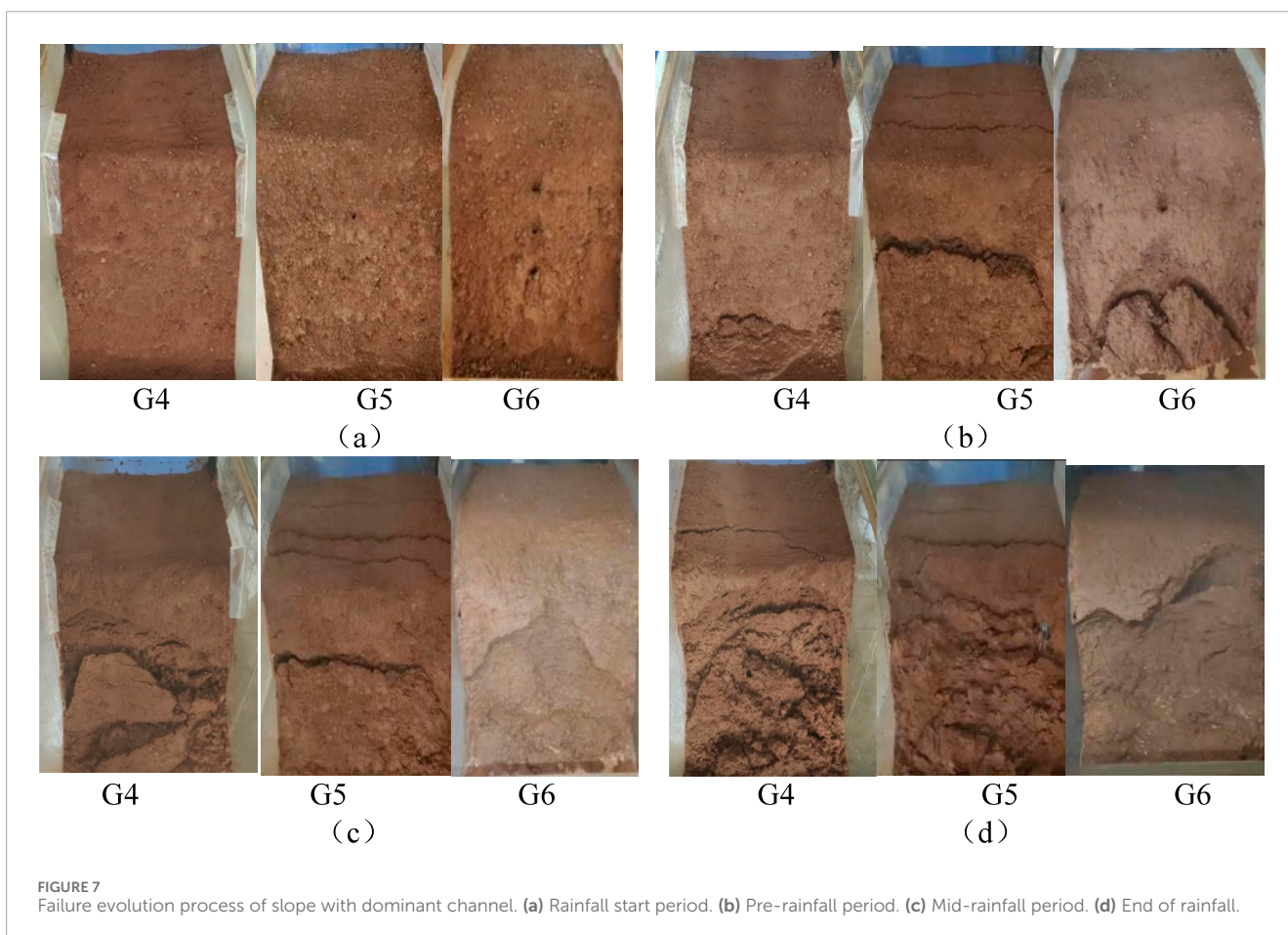
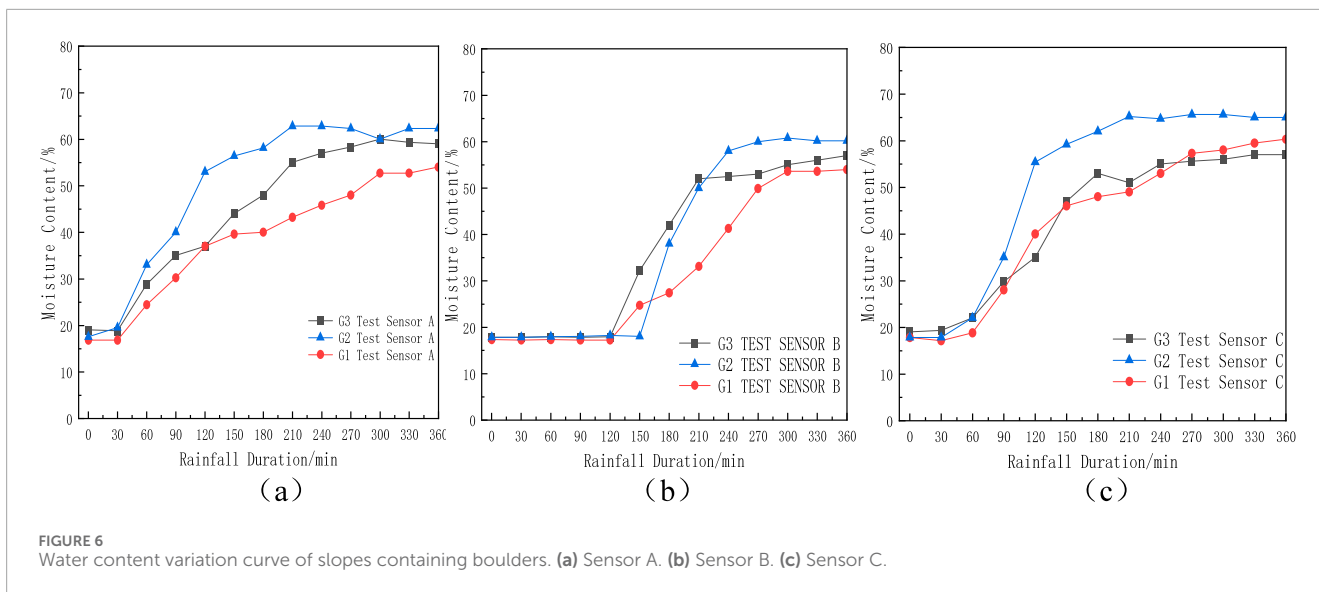
During the middle stage of rainfall, surface soil gradually approached saturation, resulting in ponding within the channels. Rainwater began to erode outward toward surrounding soil. Pore water pressure and earth pressure increased progressively, further expanding cracks along the channels and forming new tension cracks near the crest. The G4 slope exhibited local surface instability and minor sliding, while the G5 slope developed new tension cracks

at the top. In the G6 slope, lower channels became fully connected, forming continuous preferential flow paths.

During the late stage, as the internal soil approached saturation, overall shear strength decreased, causing failure to evolve from local to large-scale instability. The G4 slope showed extensive instability along the surface and toe. In the G5 slope, traction-type tensile failure developed at the top, and in G6, slip surfaces were clearly defined with the most significant landslide. These results indicate that dominant channels accelerate slope instability, and an increased number of channels promotes larger-scale landslides and more distinct slip surfaces.

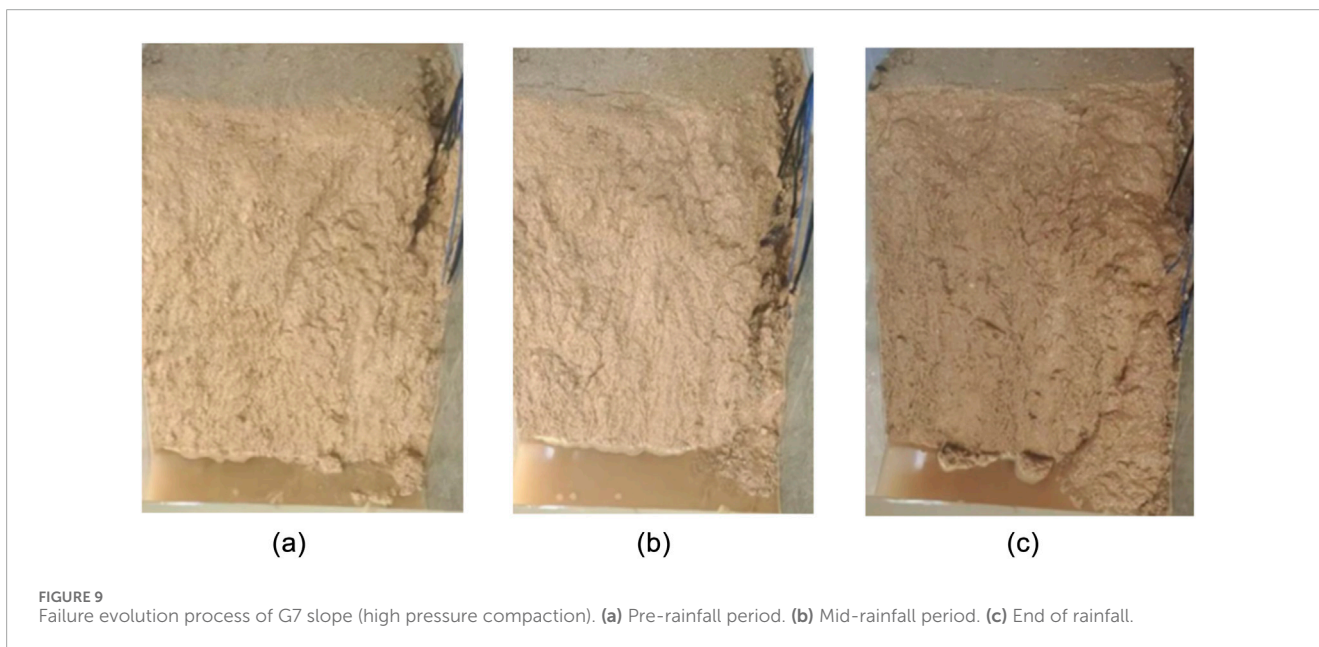
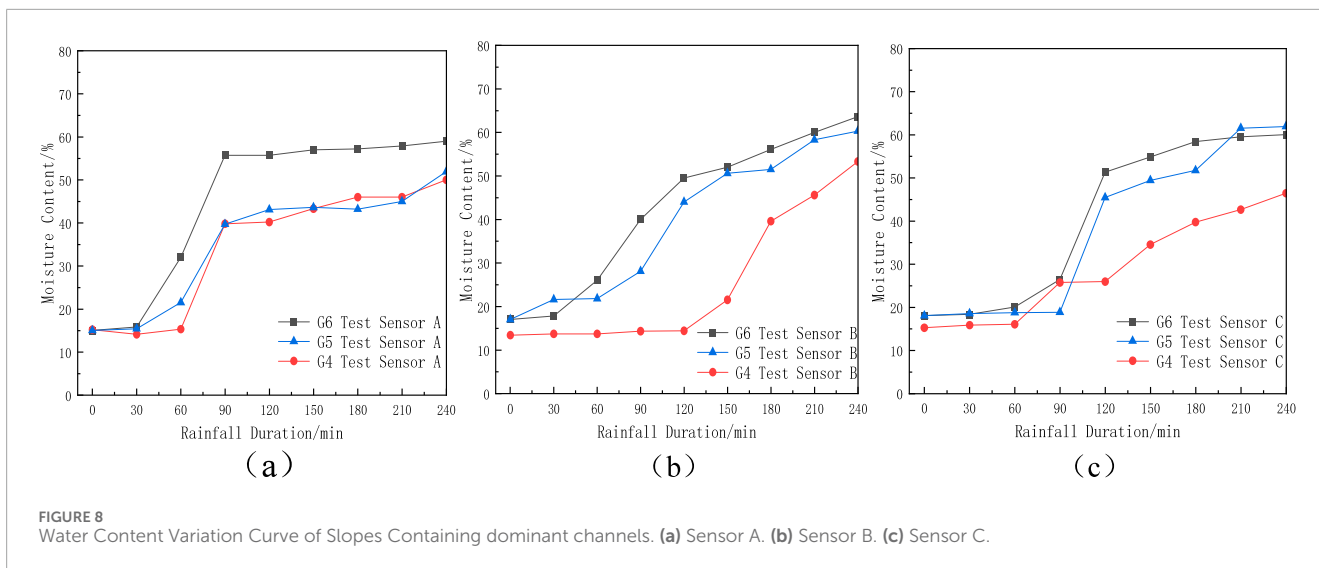
3.2.2 Influence of dominant channels on water content

As shown in Figure 8, the G6 slope with three dominant channels exhibits the highest water content. In the G5 and G4 tests, due to a dominant channel near location C in G5, the



difference in water content at location A is small; however, at locations B and C, G5 shows significantly higher moisture than G4. This demonstrates that dominant channels accelerate downward

rainwater infiltration, leading to faster soil saturation and earlier slope failure. Furthermore, the greater the number of dominant channels, the faster the increase in soil water content.



3.3 Influence of soil compaction on the stability of granite residual soil slope with boulders

3.3.1 Influence of soil compaction on failure mode

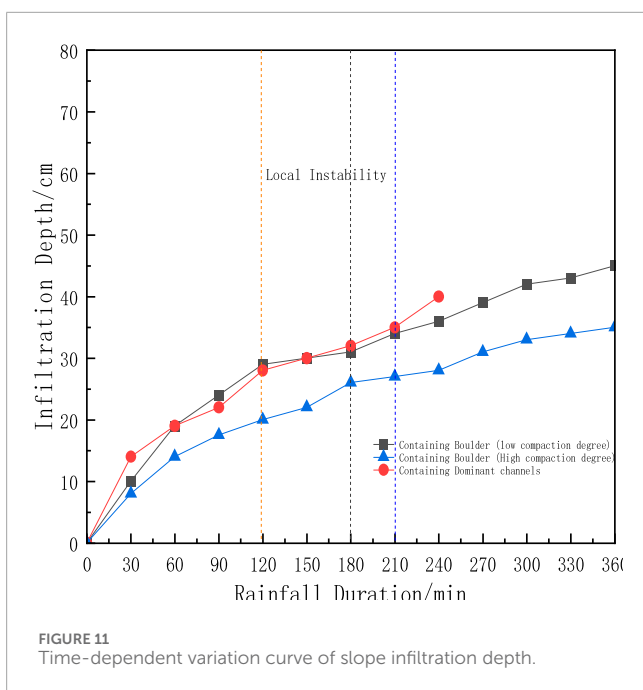
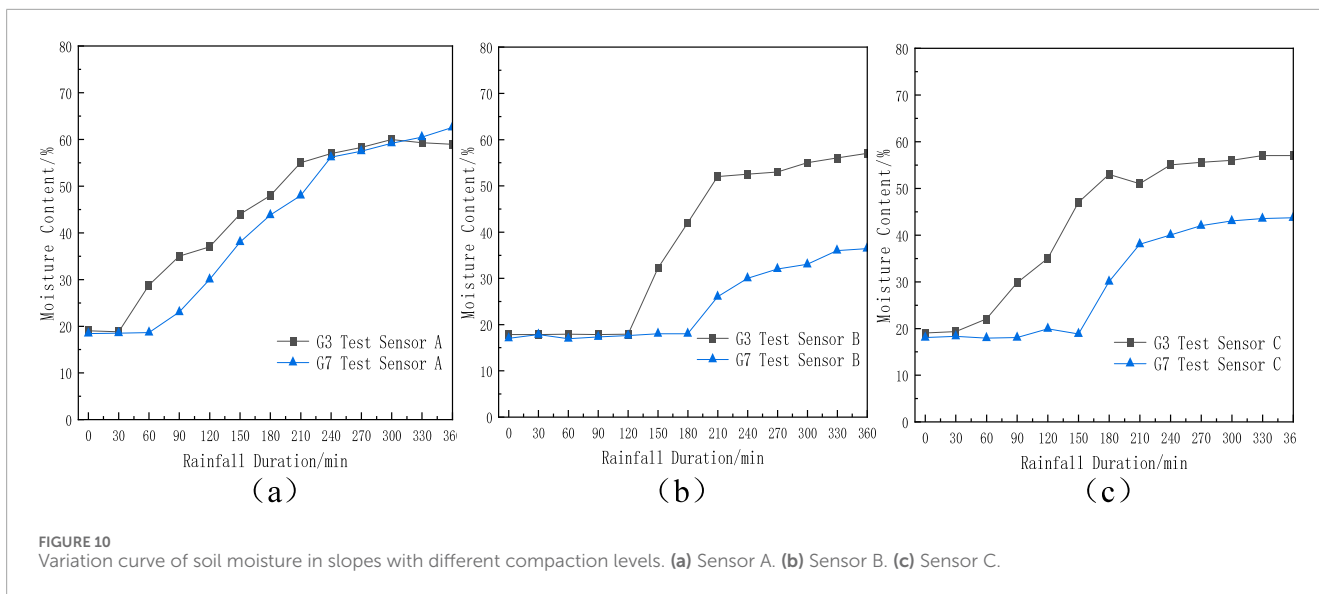
As shown in Figure 9, during 360 min of continuous rainfall in the G7 test, no significant landslide occurred, though substantial ponding was observed at the slope toe. Compared with G3, higher compaction in G7 reduced soil porosity and slowed rainwater infiltration, delaying overall instability and promoting water accumulation at the surface. Rainwater flowed along dominant paths, causing erosion at the slope toe. High-pressure compaction effectively delays overall slope instability but promotes water accumulation at the toe, where soil particles gradually slide downward.

3.3.2 Influence of soil compaction on water content

As shown in Figure 10, location A, close to the surface, shows similar moisture content in G3 and G7. Locations B and C, deeper in the slope, experience slower infiltration in the high-compaction G7 slope, while low-compaction G3 allows easier infiltration. Therefore, soil compaction directly influences internal moisture content and rainwater infiltration rate, which in turn governs slope instability progression.

4 Discussion on influencing factors

As shown in Figure 11, rainfall infiltration tests on slopes with boulders, dominant channels, and varying compaction levels were analyzed to monitor dynamic rainwater infiltration depth



beneath the slope crest. Infiltration depth–time curves were plotted according to the timing of local instability events.

Comparison of local instability times indicates that slopes with dominant channels exhibit the highest infiltration rates and earliest onset of instability, followed by slopes with low-compaction containing boulders, while high-compaction slopes show the slowest infiltration and latest instability. This sequence highlights the fundamental role of internal heterogeneity in controlling subsurface hydrological behavior.

Dominant channels act as preferential seepage pathways, rapidly transmitting surface water into the slope interior and connecting surface runoff with potential sliding zones. This sharply increases pore water pressure, accelerates saturation, and reduces effective stress, resulting in rapid local instability and large-scale landslides.

Boulders create local seepage barriers, forcing rainwater to bypass them and concentrate along their periphery, forming secondary preferential seepage paths. This locally enhances pore water pressure and initiates micro-failures. Although boulder-induced infiltration acceleration is weaker than that caused by dominant channels, their presence significantly alters hydraulic gradients and promotes progressive failure under long-duration rainfall.

High-pressure compaction reduces porosity and permeability, increasing hydraulic resistance and delaying wetting front propagation. Smaller pore space limits infiltration rate, and stronger interparticle contact enhances cohesion and internal friction, resulting in slower pore pressure buildup, lower saturation, and delayed failure onset. Compaction thus serves as an engineering control parameter for slope stabilization.

Overall, the synergistic effect of boulders and dominant channels reshapes the internal seepage field, producing a nonuniform hydraulic response. Direct and secondary preferential paths accelerate wetting front migration and induce localized stress redistribution, leading to a transition from local failure to overall instability. High compaction counterbalances these effects by suppressing rapid infiltration and reducing strength degradation. Therefore, the spatial distribution of structural heterogeneities and soil compaction jointly determine the dynamic response and failure pattern of granite residual soil slopes under rainfall conditions.

From an engineering application perspective, the identified coupling mechanisms between boulders, dominant seepage channels, and soil compaction can provide guidance for predictive and preventive slope management in granite residual soil regions. The results suggest that monitoring the spatial distribution of preferential flow paths and the presence of boulders can help identify slopes with a higher susceptibility to rapid infiltration and localized failure. Engineering measures, such as minimizing the development of dominant channels through surface drainage control, strategically placing boulders or barriers to disrupt secondary preferential flow paths, and optimizing compaction during slope construction, can effectively delay saturation and reduce the rate of strength degradation. Furthermore, the experimental infiltration data and

observed failure patterns could inform site-specific predictive rainfall thresholds, allowing engineers to estimate the rainfall intensity and duration that may trigger instability under given slope conditions. In practice, combining these design-based mitigation strategies with routine monitoring of pore pressure and surface runoff can significantly enhance the safety and resilience of slopes in humid climates.

5 Conclusion

The following are the main conclusions from the study:

1. The spatial distribution of boulders exerts a significant control on slope seepage paths, directly influencing both the development scale and the rate of slope instability. As boulders migrate within the slope, local stress concentrations intensify, causing pronounced deflection of the seepage paths and promoting soil softening. The results indicate that the closer a boulder is positioned to the slope surface, the shorter the onset time of local slope instability, accompanied by a substantial increase in landslide volume.
2. As conduits for rapid seepage within the slope, dominant channels significantly enhance rainwater infiltration efficiency. This non-uniform seepage structure accelerates soil saturation, and both the number and spatial distribution of dominant channels strongly influence the evolution of landslide scale. An increase in the number of dominant channels promotes faster lateral and vertical diffusion of rainwater, leading to a rapid reduction in effective stress and consequently more pronounced slope instability.
3. Although both dominant channels and boulders can promote local slope instability, their mechanisms of action are fundamentally different. Dominant channels create direct seepage paths, allowing rainwater to rapidly infiltrate the soil mass, whereas boulders alter the existing seepage field, inducing the formation of secondary preferential flow networks. Under identical rainfall conditions, the enhancement of soil saturation rate by dominant channels is significantly greater than the path-altering effect caused by boulders, resulting in a more pronounced instability response.
4. Soil compaction is a key factor controlling the rate of rainwater infiltration and is positively correlated with slope stability. Highly compacted soils exhibit lower permeability and higher shear strength, effectively slowing the infiltration process. Therefore, optimizing soil compaction is an effective engineering measure to enhance the anti-seepage performance of slopes.

Data availability statement

The raw data supporting the conclusions of this article will be made available by the authors, without undue reservation.

Author contributions

XZ: Conceptualization, Writing – review and editing, Investigation, Software. CX: Data curation, Supervision, Writing – original draft, Methodology. LZ: Writing – review and editing, Formal Analysis, Validation, Project administration. ZH: Writing – review and editing, Funding acquisition, Resources, Visualization.

Funding

The author(s) declared that financial support was received for this work and/or its publication. The research was supported by Key Fields Special Project for Ordinary Universities in Guangdong Province (2023ZDZX4113); Guangdong Province Vocational Education Teaching Reform and Practice Project (2023JG548); Research Project of Guangzhou Panyu Vocational and Technical College (2021KJ06); the Science and Technology Program of Guangzhou Construction Engineering Co., Ltd., Guangzhou, Guangdong 510030, China ([2022] -KJ002, [2023]-KJ050), [2024] -KJ075, [2022] -KJ015, 2023Y-KJ02). The authors declare that this study received funding from Guangzhou Construction Engineering Co., Ltd. The funder was not involved in the study design, data collection, analysis, interpretation of data, the writing of this article, or the decision to submit it for publication.

Conflict of interest

The author(s) declared that this work was conducted in the absence of any commercial or financial relationships that could be construed as a potential conflict of interest.

Generative AI statement

The author(s) declared that generative AI was not used in the creation of this manuscript.

Any alternative text (alt text) provided alongside figures in this article has been generated by Frontiers with the support of artificial intelligence and reasonable efforts have been made to ensure accuracy, including review by the authors wherever possible. If you identify any issues, please contact us.

Publisher's note

All claims expressed in this article are solely those of the authors and do not necessarily represent those of their affiliated organizations, or those of the publisher, the editors and the reviewers. Any product that may be evaluated in this article, or claim that may be made by its manufacturer, is not guaranteed or endorsed by the publisher.

References

- Abgrami, A., Zhang, W., Mao, H., and Wang, L. (2025). GIS-based comparative landslide susceptibility mapping for Kelardasht county with ANN, SVM and RF models. *Civ. Geoenviron. Lett.*, 2(1), e100028. doi:10.7733/cgel.2024.e100028
- Bai, H., Feng, W., Yi, X., Fang, H., Wu, Y., Deng, P., et al. (2021). Group-occurring landslides and debris flows caused by the continuous heavy rainfall in June 2019 in Mibei Village, Longchuan County, Guangdong Province, China. *Nat. Hazards* 108 (3), 3181–3201. doi:10.1007/s11069-021-04819-1
- Bai, H., Feng, W. k., Li, S. q., Ye, L. z., Wu, Z. t., Hu, R., et al. (2022). Flow-slide characteristics and failure mechanism of shallow landslides in granite residual soil under heavy rainfall. *J. Mt. Sci.* 19 (6), 1541–1557. doi:10.1007/s11629-022-7315-8
- Bravo-Zapata, M., Muñoz, E., Lapeña-Mañero, P., Montenegro-Cooper, J. M., and King, R. W. (2022). Analysis of the influence of geomechanical parameters and geometry on slope stability in granitic residual soils. *Appl. Sciences-Basel* 12 (11), 5574. doi:10.3390/app12115574
- Chen, J. (2025). Experimental study on granite-weathered crust landslides with different residual layer thicknesses under heavy rainfall. *Earth Surf. Dyn.* 13 (5), 861–873. doi:10.5194/esurf-13-861-2025
- Danesh, N., Taghizadeh, A., Valinejad, M., and Kouhdaragh, M. (2025). Laboratory Investigation of Creep Behavior in High-high-pcity LooselSoilssunder Constnt ShearsStress. *Cis. Geoenviron. Lett.* 2 (1), e100025.
- Ding, J., Wang, S., Huang, H., Pan, F., Wu, Y., Gu, Y., et al. (2023). Prediction model of residual soil shear strength under dry-wet cycles and its uncertainty. *Water* 15 (22), 3931. doi:10.3390/w15223931
- Dou, H., Xie, S. h., Jian, W. b., Wang, H., and Guo, C. x. (2024). Characteristics of preferential flow suffosion of soil-rock interface in spherical weathered granite slopes. *Rock Soil Mech.* 45 (4), 950–960. doi:10.26599/rsm.2024.9435644
- Feng, W., Bai, H., Lan, B., Wu, Y., Wu, Z., Yan, L., et al. (2022). Spatial-temporal distribution and failure mechanism of group-occurring landslides in Mibei village, Longchuan County, Guangdong, China. *Landslides* 19 (8), 1957–1970. doi:10.1007/s10346-022-01904-9
- Guo, Y., Li, S., Zhang, J., Wang, B., and Gao, Y. (2023). Study on the seepage mechanism of rainwater on granite residual soil cut slopes. *Adv. Civ. Eng.* 2023, 1–7. doi:10.1155/2023/1259527
- Hang, L., Gao, Y., van Paassen, L. A., He, J., Wang, L., and Li, C. (2023). Microbially induced carbonate precipitation for improving the internal stability of silty sand slopes under seepage conditions. *Acta Geotech.* 18 (5), 2719–2732. doi:10.1007/s11440-022-01712-4
- Jian, W. (2020). Experimental study on wetting front migration induced by rainfall infiltration in unsaturated eluvial and residual soil. *Rock Soil Mech.* 41 (4), 1123–1133. doi:10.16285/j.rsm.2019.1730
- Lai, H., Ding, X. Z., Cui, M. J., Zhou, Y. J., Zheng, J. J., and Chen, Z. B. (2025). Premix-spray biomineralization method for anti-disintegration improvement of granite residual soil. *Acta Geotech.* 20 (3), 1251–1265. doi:10.1007/s11440-024-02449-y
- Lan, B., Jia, B., Wu, Y., Yi, X., Feng, W., and Li, Y. (2025). Strength characteristics in saturation process and rainfall-induced landslide failure mechanism of granite residual soil. *Front. Earth Sci.* 13, 1578923. doi:10.3389/feart.2025.1578923
- Li, S., Niu, Y., Wang, B., Gao, Y., and Zhu, Y. (2022). Influence of rainfall infiltration on stability of granite residual soil high slope. *Math. Problems Eng.* 2022, 1–7. doi:10.1155/2022/1920403
- Li, R., Fu, W., Siyi, J., Minning, H., and Hongjian, P. (2025). Field-based investigation of failure modes and thresholds of granite residual soil slopes under heavy rainfall conditions. *Plos One* 20 (2), e0317836. doi:10.1371/journal.pone.0317836
- Ling, J., Li, X., Lin, S., Cen, Y., and Li, C. (2023). Laboratory study on entire range suction measurement and microstructure change of granite residual soil. *Transp. Res. Rec.* 2677 (10), 191–203. doi:10.1177/03611981231160546
- Liu, W., Ouyang, G., Luo, X., Luo, J., Hu, L., and Fu, M. (2020). Moisture content, pore-water pressure and wetting front in granite residual soil during collapsing erosion with varying slope angle. *Geomorphology* 362, 107210. doi:10.1016/j.geomorph.2020.107210
- Liu, X., Zhang, X., Kong, L., Wang, G., and Liu, H. (2022). Formation mechanism of collapsing gully in southern China and the relationship with granite residual soil: a geotechnical perspective. *Catena* 210, 105890. doi:10.1016/j.catena.2021.105890
- Liu, W., Cui, Y., Ouyang, G., and Lyu, Z. (2023). An experimental study on influence of grain-size composition on collapsing erosion of granite residual soil. *Catena* 223, 106949. doi:10.1016/j.catena.2023.106949
- Liu, W., Zeng, B., Wang, T., and Duan, J. (2024). Effects of soil crust on the collapsing erosion of colluvial deposits with granite residual soil. *J. Mt. Sci.* 21 (8), 2579–2591. doi:10.1007/s11629-023-8467-x
- Mao, Q., Guo, K., Zhang, J., Xiao, G., Du, J., Cheng, X., et al. (2024). Response of granite residual soil slopes under dry-wet cycles. *Front. Earth Sci.* 11, 1333668. doi:10.3389/feart.2023.1333668
- Moazafarbaygi, A., and Asghari-Kalajahi, E. (2024). Assessment of soil liquefaction Potential in Eastern Miandoab by FieldData dnd Empirical Relationships. *Civ. Geoenvironment Lett.* 1 (1), e100012.
- Pan, Y. (2020). A study on the rainfall infiltration of granite residual soil slope with an improved green-ampt model. *Rock Soil Mech.* 41 (8), 2685–2692. doi:10.16285/j.rsm.2019.1525
- Pradhan, A., and Kim, Y. (2015). Application and comparison of shallow landslide susceptibility models in weathered granite soil under extreme rainfall events. *Environ. Earth Sci.* 73 (9), 5761–5771. doi:10.1007/s12665-014-3829-x
- Rahardjo, H., Satyanaga, A., and Leong, E. C. (2023). Role of dual porosity in rainfall-induced slope failure. *Eng. Geol.* 320, 106–118.
- Shu, R. (2023). Mechanical behavior of granite residual soil under unloading and increasing pore water pressure. *Rock Soil Mech.* 44 (2), 473–482. doi:10.16285/j.rsm.2022.0829
- Tan, D., Xu, X., Wang, L., Xu, J., and Shi, Q. (2025). Deformation evolution and failure mechanism of rainfall-induced granite residual soil landsliding event in Northern Guangdong, China. *Landslides* 22 (3), 925–941. doi:10.1007/s10346-024-02403-9
- Tao, Y., He, Y., Duan, X., Zou, Z., Lin, L., and Chen, J. (2017). Preferential flows and soil moistures on a Benggang slope: determined by the water and temperature co-monitoring. *J. Hydrology* 553, 678–690. doi:10.1016/j.jhydrol.2017.08.029
- Wang, R., Li, H., Chen, Z., Liu, F., Wei, M., Liu, F., et al. (2023). Strength and mechanism of granite residual soil strengthened by microbial-induced calcite precipitation technology. *Appl. Sciences-Basel* 13 (15), 8863. doi:10.3390/app13158863
- Wang, Y., Li, S. K., Li, Z. Y., and Garg, A. (2023). Exploring the application of the MICP technique for the suppression of erosion in granite residual soil in Shantou using a rainfall erosion simulator. *Acta Geotech.* 18 (6), 3273–3285. doi:10.1007/s11440-022-01791-3
- Wang, Z., Zheng, C., Zhang, L., Xiong, K., and Li, Z. (2023). Research progress on stability analysis methods of granite residual soil slope. *E3S Web Conf.* 375, 01056. doi:10.1051/e3sconf/202337501056
- Wang, Y., Li, M., Peng, H., Kang, J., Guo, H., Luo, Y., et al. (2025). Improvement of unconfined compressive strength in granite residual soil by Indigenous microorganisms. *Sustainability* 17 (15), 6895. doi:10.3390/su17156895
- Wen, T., Luo, Y., Tang, M., Chen, X., and Shao, L. (2024). Effects of representative elementary volume size on three-dimensional pore characteristics for modified granite residual soil. *J. Hydrology* 643, 132006. doi:10.1016/j.jhydrol.2024.132006
- Wu, S., Zhao, R., Liao, L., Yang, Y., Wei, Y., and Wei, W. (2022). Failure mode of rainfall-induced landslide of granite residual soil, southeastern Guangxi Province, China. *Earth Surf. Dyn.* 10 (6), 1079–1096. doi:10.5194/esurf-10-1079-2022
- Xu, J. (2023). Failure process of saturated granite residual soil slope: a 3D viscoelastic-plastic finite element modeling approach with nonstationary parameter creep. *Bull. Eng. Geol. Environ.* 82 (7), 276. doi:10.1007/s10064-023-03298-x
- Yu, X., Zhao, T., Gong, B., and Tang, C. (2023). Failure mechanism of boulder-embedded slope under excavation disturbance and rainfall. *Bull. Eng. Geol. Environ.* 82 (9), 347. doi:10.1007/s10064-023-03369-z
- Zhao, L., Zhang, Z., Wang, S., Qiao, N., and Lv, G. (2024). Investigation on the large-deformation instability characteristics of solitary Boulder slopes by material point method. *Arabian J. Sci. Eng.* 49 (4), 5531–5546. doi:10.1007/s13369-023-08429-w